Cancer Nano (2013) 4:81–89
DOI 10.1007/s12645-013-0039-2

ORIGINAL PAPER

# Surface plasmon-enhanced Ag/CuS nanocomposites for cancer treatment

**Chang Yang · Lun Ma · Xiaoju Zou · Guangya Xiang · Wei Chen**

Received: 10 April 2013 / Accepted: 5 May 2013 / Published online: 18 May 2013


**Abstract** Photothermal therapy (PTT) for cancer treatment is the use of heat between 41 and 45 °C to damage cancer cells. As a new type of transducer agent for PTT of cancer, CuS nanoparticles have several advantages. The most favorable features are the low cost, simple, and easy preparation and small size for targeting. However, the CuS nanoparticle PTT efficacy needs to be improved for practical applications. In this study, the CuS nano-PTT efficiency is enhanced via the local field enhancement from Ag nanoparticle surface plasmon coupling. The results show that absorbance of CuS nanoparticles in Ag/CuS nanocomposites is enhanced about four times by Ag nanoparticle surface plasmon coupling. Consequently, the PTT efficacy is enhanced and a power of 0.6 W/cm$^2$ with a 980-nm laser is sufficient for Ag/CuS nano-PTT activation for cancer treatment in vitro observations.

**Keyword** Photothermal therapy · Ag/CuS nanocomposites · Surface plasmon resonance · Local field enhancement · Cancer treatment

## 1 Introduction

Cancer remains one of the most deadly and challenging diseases in the world. In 2008, 7.6 million people died of cancer. Deaths from cancer worldwide are projected to continue rising, with an estimated 13.1 million deaths in 2030, according to the WHO Cancer Fact Sheet (http://www.who.int/mediacentre/factsheets/fs297/en/index.html). To fight the battle of cancer, more and better diagnostic and treatment modalities must be developed.

As a relatively noninvasive and gentle alternative for cancer treatment, hyperthermia is gaining increasing attention (Huang et al. 2006a; Huff et al. 2007). Hyperthermia is commonly defined as heating tissue to a temperature in the range 41–45 °C for tens of minutes (Svaasand et al. 1990; Zee 2002). Tumors are selectively destroyed in this temperature range because of their reduced heat tolerance compared to normal tissue, which is due to their poor blood supply (Huang et al. 2008). On one hand, hyperthermia can induce irreversible cell damage by loosening cell membranes and denaturing proteins (Huff et al. 2007; Huang et al. 2008). On the other hand, as an adjuvant therapy with chemotherapy and radiotherapy, under mild temperature increases, hyperthermia can promote the development of both perfusion and reoxygenation in tumor tissues (Rau et al. 2000; Song et al. 1996), thereby increasing the efficacy of chemotherapy and radiotherapy, respectively. Several methods have been developed for the delivery of thermal energy in a non-topical manner, such as microwave irradiation, radiofrequency pulses, and ultrasound. They can penetrate deep into tissue but may require a high fluence because of their diffuse nature, possibly producing undesirable hyperthermic effects in surrounding tissues (Li and Gu 2010). Laser irradiation at near-infrared (NIR) frequencies can penetrate tissues with sufficient intensity and higher spatial precision for inducing localized hyperthermia (Castrén-Persons et al. 1991; Chen et al. 1997), but effective mechanisms are needed to transduce light energy into heat and to discriminate unhealthy from healthy cells (Huff et al. 2007). One promising approach is to introduce the photothermal agents in the near-infrared region.

Photothermal therapies (PTT) for cancer have been widely investigated as a minimally invasive oncological treatment

C. Yang · L. Ma · X. Zou · W. Chen (✉)
Department of Physics, The University of Texas at Arlington, Arlington, TX 76019-0059, USA
e-mail: weichen@uta.edu

C. Yang · G. Xiang (✉)
Department of Pharmacy, Tongji Medical College, Huazhong University of Science and Technology, Wuhan, Hubei 430032, China
e-mail: gyxiang1968@hotmail.com

strategy in which photon energy is converted into heat to induce cellular destruction (O'Neal et al. 2004a; Rozanova and Zhang 2009; Huang and El-Sayed 2011). With the tremendous development of nanotechnology, gold nanostructures such as nanospheres (El-Sayed et al. 2006; Khlebtsov et al. 2006), nanorods (Dickerson et al. 2008; Huang et al. 2006b), nanoshells (O'Neal et al. 2004b; Loo et al. 2005), nanocages (Chen et al. 2005; Hu et al. 2006), as well as carbon nanotubes (Zhou et al. 2009; Robinson et al. 2010) have been investigated extensively for PTT therapy in the near-infrared region. CuS nanoparticles have a broad absorption from 700 to 1,100 nm, and we first demonstrated that the interaction of CuS nanoparticles with near-infrared light can generate heat that can be harnessed for PTT of cancer cells (Li et al. 2010; Zhou et al. 2010). As a new type of agent for photothermal treatment of cancer, CuS nanoparticles have several advantages such as the low cost, simple, and easy preparation and small size for targeting (Li et al. 2010). However, the PTT efficiency using CuS nanoparticles as transducers is low and needs to be improved for practical applications (Tian et al. 2011; Lakshmanan et al. 2012). Here, we investigate the enhancement of CuS nanoparticle PTT efficacy by Ag nanoparticle surface plasmon coupling in Ag/CuS nanocomposites for cancer treatment. A surface plasmon is a localized electromagnetic field at the metal dielectric interface (Englebienne et al. 2003). Surface plasmons can lead to significant electric field enhancement near the surface and thus increase the rate of any processes that depend on the field intensity. The field enhancement due to surface plasmon resonance is predicted to be ~1,000 times larger than the incident field and, therefore, it can be used to increase any light excitation or transition processes at the interfaces (Aslan et al. 2005; Lakowicz 2001). Because of the localized field amplification that occurs, excitation of surface plasmons in metal nanoparticles placed on a semiconductor might be expected to enhance optical absorption of incident photons within the semiconductor region near each nanoparticle. We have studied and observed the absorption enhancement of CuS by surface plasmon in Au/CuS nanocomposites and the application of Au/CuS for cancer treatment with improved efficacy (Lakshmanan et al. 2012). Here, we report the observations on Ag/CuS nanocomposites for surface plamosn enhancement and the application for Ag/CuS nanocomposites for cancer treatment by in vitro studies. We are interested in Ag/CuS nanocomposites because it has been reported that among the three metals (Ag, Au, Cu) with efficient plasmon resonances, Ag exhibits the highest efficiency of plasmon excitation (Evanoff and Chumanov 2005). Moreover, Ag is much cheaper than Au. Therefore, as photothermal transducer agents for cancer treatment, Ag/CuS nanocomposites might have a higher potential and better market than Au nanostructures and Au/CuS nanocomposites.

## 2 Materials and methods

### 2.1 Materials

Copper(II) chloride dehydrate ($CuCl_2\ 2H_2O$), sodium sulfide ($Na_2S$), sodium citrate, sodium carbonate ($Na_2CO_3$), thiobenzoic acid, copper(II) nitrate hemi(penta hydrate) ($Cu(NO_3)_2\ 2.5H_2O$), silver perchlorate anhydrous ($AgClO_4$), hexadecyltrimethylammonium bromide (CTAB), and L-ascorbic acid were purchased from Sigma-Aldrich (MO, USA). Sodium borohydride ($NaBH_4$) was obtained from Acros Organics (NJ, USA). Nickel nitrate ($Ni(NO_3)_2\ 6H_2O$) was purchased from Alfa Aesar.

### 2.2 Preparation of Ag nanoparticles

Ag nanoparticles were grown using the seeded growth method according to the literature (Sun et al. 2009). Specifically, the seeds were made by the addition of a freshly prepared, ice-cold 0.01 M $NaBH_4$ solution (600 μL, 0.006 mmol) into a mixture solution composed of 0.01 M $AgClO_4$ (250 μL, 0.0025 mmol) and 0.1 M CTAB (7.5 mL, 0.75 mmol). The resultant solution was mixed by rapid inversion for 2 min and was then kept at room temperature for 1 h before use. The growth solution was prepared by the sequential addition of 0.1 M CTAB (6.4 mL, 0.64 mmol), 0.01 M $AgClO_4$ (800 μL, 0.008 mmol), and 0.1 M ascorbic acid (3.8 mL, 0.38 mmol) into water (32 mL). The CTAB-stabilized seed solution was diluted ten times with water. The diluted seed solution was then added into the growth solution for the growth of Ag nanoparticles. The resultant solution was mixed by gentle inversion for 10 s and then left undisturbed overnight.

### 2.3 Synthesis of Ag/CuS nanocomposites

Nickel thiobenzoate ($(PhCOS)_2Ni$) is used as the sulfur source for Ag/CuS synthesis and is synthesized based on the synthetic route reported in the literature (Sun et al. 2009). Sodium thiobenzoate was first prepared by mixing together $Na_2CO_3$ (211.98 mg, 2.00 mmol), thiobenzoic acid (PhCOSH, 520 μL, 4.40 mmol), and water (1 mL) at room temperature. The resultant concentrated PhCOSNa solution was then added into an aqueous 0.4 M $Ni(NO_3)_2$ (10 mL, 2.00 mmol) solution to produce nickel thiobenzoate ($(PhCOS)_2Ni$). The dark red precipitate was washed with water and dried under ambient conditions.

To prepare Ag/CuS nanocomposites, $(PhCOS)_2Ni$ (2 mg, 0.006 mmol) was dissolved in the Ag nanoparticle dispersion (10 mL), followed by the addition of 0.01 M $Cu(NO_3)_2$ solution. The concentration of $Cu^{2+}$ in the solution was controlled to be 300 μM. The resultant mixture solution was transferred into an autoclave and heated at 140 °C for

3 h, and then cooled down to room temperature. The prepared nanoparticle solution was dialyzed for 3 h to remove all the unreacted chemicals.

### 2.4 Preparation of CuS nanoparticles

CuS nanoparticles were prepared as follows: to 100 mL of an aqueous solution containing $CuCl_2$(0.1 mmol, 17.05 mg) and sodium citrate (0.068 mmol, 20 mg), 1 mL of sodium sulfide solution ($Na_2S$, 0.1 M) was added while stirring at room temperature. The pale blue $CuCl_2$ solution turned dark brown immediately upon the addition of sodium sulfide. After 5 min, the reaction mixture was heated to 90 °C and stirred for 15 min, until dark green solution was obtained. The citrate-coated CuS nanoparticles were obtained and stored at 4 °C.

### 2.5 Characterization of Ag/CuS nanocomposites

Ag/CuS nanocomposites in solution were placed onto holey carbon-covered copper grids for high-resolution transmission electron microscope (HRTEM) observation. The HRTEM images of the particles were obtained with a JEOL JEM-2100 electron microscope (Tokyo, Japan) with accelerating voltage of 200 kV. The absorption spectra were recorded using a Shimadzu UV-2450 UV–Vis spectrophotometer (Kyoto, Japan). The luminescence excitation and emission spectra were measured using a Shimadzu RF-5301PC fluorescence spectrophotometer (Kyoto, Japan). The Ag and Cu element analysis were operated on the PerkinElmer ELAN DRC II ICP Mass Spectrometer system (ICP-MS) with an autosampler.

### 2.6 Photothermal effect in aqueous solution

For measuring temperature change mediated by CuS nanoparticles or Ag/CuS nanocomposites, 980 nm near-infrared light (Opto Engine LLC) at an output power of 0.6 W/cm$^2$ was delivered through a cuvette containing the nanoparticles (1 mL). The Cu concentration in both Ag/CuS nanocomposites and CuS nanoparticles was 13.912 mg/L. The temperature was measured by a digital thermometer (Fisher Scientific "Traceable") over a period of 20 min. Water was used as a control.

### 2.7 In vitro fluorescence imaging

In this study, prostate cancer PC-3 cells were used to evaluate the fluorescence imaging of Ag/CuS nanocomposites. PC-3 were cultured in F-12K medium supplemented with 10 % fetal bovine serum and 1 % penicillin–streptomycin solution, and incubated at 37 °C in a water-saturated incubator with 5 % $CO_2$. The cells were treated with 10 % of original Ag/CuS nanocomposites for 24 h. The Ag and Cu concentration of original Ag/CuS nanoparticles were 46.606 and 13.912 mg/L, respectively. Fluorescence imaging was done on the following day using an Olympus 1X71 inverted fluorescence microscope.

### 2.8 Time course of cellular uptake by PC-3 cells

The time course of cellular uptake was also carried out on prostate cancer PC-3 cells. Aliquots of the cultured cells were incubated with 5 % of original Ag/CuS nanocomposites for 10 min, 30 min, 1 h, 2 h, 4 h, and 8 h at 37 °C under 5 % $CO_2$ in the 1.5 mL centrifuge tubes. After incubation, the cells were washed two times with PBS. All the imaging results were examined by an Olympus 1X71 Inverted Microscope (Tokyo, Japan).

### 2.9 In vitro photothermal ablation of cancer cells with Ag/CuS nanocomposites

The cells were cultured as described in the above section and incubated with 2.5, 5, and 10 % of the original Ag/CuS nanoparticle solution at 37 °C and 5 % $CO_2$ for 4 h. After incubation was completed, the culture medium with nanoparticles were removed and resupplied with fresh medium. The cells were then irradiated with a 980-nm NIR laser (Opto Engine LLC) at an output power of 0, 0.6, 1.2, or 1.8 W/cm$^2$ for 5 min. Fluorescence imaging was used to see the number of living and dead cells after photothermal

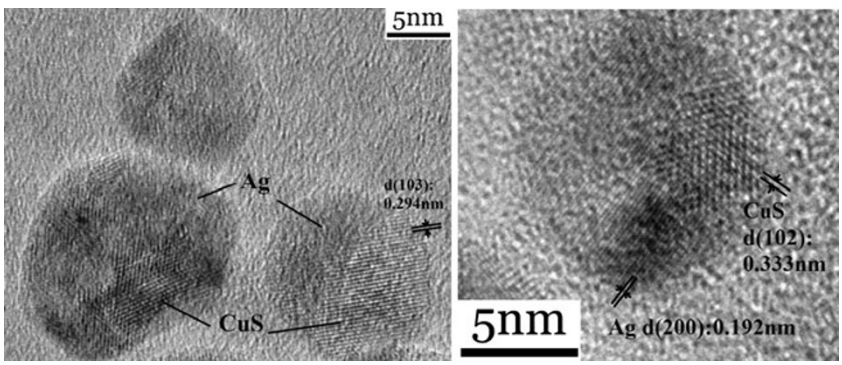


**Fig. 1** HRTEM images of Ag/CuS nanocomposites. The *d*-spacing of 0.192, 0.294, and 0.333 nm correspond to the (200) lattice planes of silver, the (103) and (102) lattice planes of copper sulfide, respectively

treatment. The live cells were stained with calcein AM and the dead cells with ethidium homodimer-1 (EthD-1), according to the manufacturer's suggested protocol (Invitrogen). The cells were imaged under an Olympus 1X71 inverted fluorescence microscope.

3-(4,5-Dimethylthiazol-2-yl)-2,5-diphenyltetrazolium-bromide (MTT) assay was also applied to estimate the photothermal effect of Ag/CuS nanocomposites. The cultured PC-3 cells were incubated with 5 and 10 % of original Ag/CuS nanocomposites for 4 h and were irradiated with a 980-nm NIR laser (Opto Engine LLC) at an output power of 0, 0.3, 0.6, or 0.9 W/cm$^2$ for 1 min. Ten microliters of 5 mg/ml MTT solution was added to each well and incubated for 4 h at 37 °C under 5 % $CO_2$. The supernatant was then removed, and the cells were lysed with 50 μL dimethyl sulfoxide. Using a microplate reader, absorbance was recorded at 570 nm to determine cell survival.

## 3 Results and discussion

The morphology of Ag/CuS nanocomposites was observed by the HRTEM as shown in Fig. 1. Most of them are spherical and their diameters are in the range of 10–20 nm. Each Ag/CuS nanocomposite nanoparticles contains both Ag and CuS nanoparticles as shown in the HRTEM images. The clear lattice fringes observed in the cores indicate the high crystallinity. The *d*-spacing of 0.192 nm corresponds to the (200) lattice planes of silver (Sharma et al. 2010; Feng et al. 2011; Kim et al. 2012), while the crystal lattice fringes with *d*-spacing of 0.294 and 0.333 nm correspond to the (102) and (103) lattice planes of copper sulfide (Wu et al. 2006; Xu et al. 2006; Zhu et al. 2005). Because Ag and CuS nanoparticles are closely packed into one nanocomposite nanoparticle which enables their interaction and the coupling of Ag surface plasmon with the *d*–*d* transition of $Cu^{2+}$ in CuS nanoparticles. It is reported that the NIR absorption in CuS nanoparticles originates from the *d*–*d* transition of $Cu^{2+}$; thus, their absorption wavelength is hardly affected by the surrounding matrix (Li et al. 2010). This property of CuS nanoparticles can largely enhance the resistance to the surrounding environment. To measure the concentration of Ag and Cu elements in the nanocomposites, ICP-MS measurements were carried out. The Ag/CuS nanocomposites contain 13.912 mg/L of Cu and 46.606 mg/L of Ag, respectively. The optical absorption spectra of Ag nanoparticles, CuS nanoparticles, Ag/CuS nanocomposites, and the mixture of Ag and CuS nanoparticles are shown in Fig. 2. The absorption shoulder around 375 nm appears in the spectra of Ag nanoparticles and the mixture of Ag and CuS nanoparticles, which is assigned to Ag absorption (Sharma et

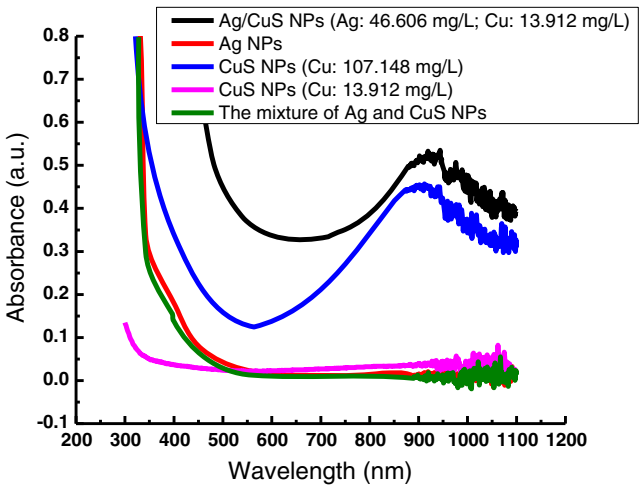


**Fig. 2** The absorption spectra of Ag nanoparticles, CuS nanoparticles, and Ag/CuS nanocomposites. The Cu concentrations of Ag/CuS nanocomposites, CuS nanoparticles, and the mixture of Ag and CuS nanoparticles are 13.912 mg/L

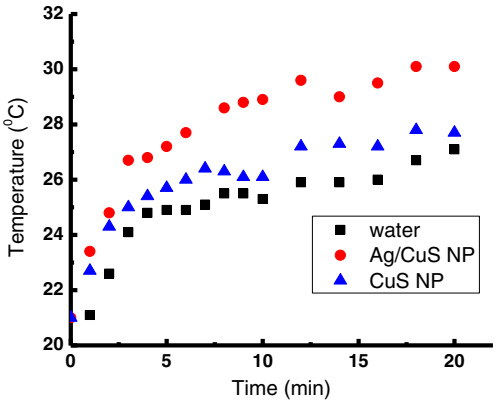


**Fig. 3** Temperature measured in the water over a period of 20 min upon exposure to 980-nm near-infrared light at an output power of 0.6 W/cm$^2$. The Cu concentration of Ag/CuS nanocomposites and CuS nanoparticles in water were 13.912 mg/L

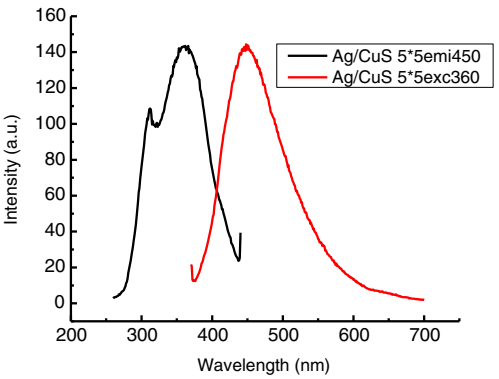


**Fig. 4** The photoluminescence spectra of Ag/CuS nanocomposites. The excitation spectrum was obtained under 450-nm emission. The emission spectrum was measured with the excitation wavelength at 360 nm. Both the slit widths of the excitation and emission were 5 nm

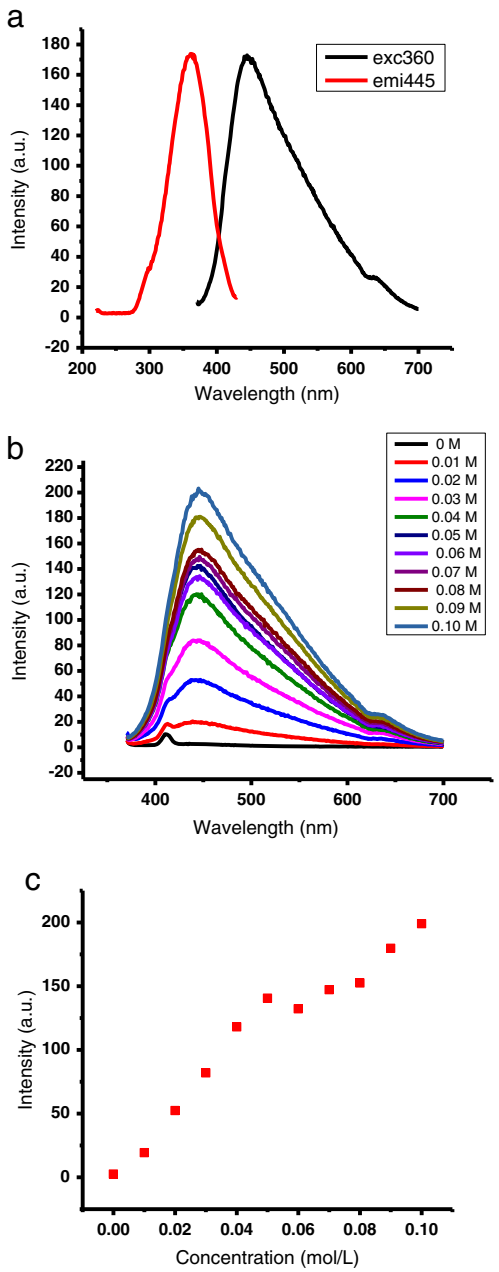


**Fig. 5** The photoluminescence of L-ascorbic acid. **a** The excitation and emission spectra of ascorbic acid; **b** the emission spectra of different concentration of ascorbic acid; **c** the relationship between the emission intensity and the concentration of ascorbic acid

al. 2010; Sohrabnezhad and Pourahmad 2012), while the broad absorption around 914 nm in Ag/CuS nanocomposites and CuS nanoparticles is assigned to CuS absorption (Li et al. 2010; Zhou et al. 2010; Tian et al. 2011; Lakshmanan et al. 2012). For the mixture of Ag and CuS nanoparticles, no enhancement was observed on the absorption of CuS nanoparticles. However, the CuS absorbance at 914 nm is enhanced almost four times in Ag/CuS nanocomposites when the Cu concentration of CuS nanoparticles and Ag/CuS nanocomposites are the same. Similar to what observed in Au/CuS nanocomposites (Lakshmanan et al. 2012), the enhancement of CuS absorption in Ag/CuS is due to the coupling of Ag nanoparticle surface plasmon with the *d*–*d* transition of $Cu^{2+}$ in CuS nanoparticles. However, the enhancement of CuS absorption in the Ag/CuS nanocomposites is higher than the plasmon enhancement by Au (2.2 times) in the Au/CuS nanocomposites (Lakshmanan et al. 2012). The TEM images also show that Ag and CuS nanoparticles are closely packed together in the nanoparticles which enable their coupling to cause the enhancement. The local field enhanced absorption intensity in Ag/CuS nanocomposites may enhance the PTT efficacy. To prove the enhancement, the photothermal effect in the aqueous solution was measured upon exposure to 980-nm NIR laser (Opto Engine LLC). Generally, the NIR region of the spectrum provides maximal penetration of light due to relatively lower scattering and absorption from the intrinsic tissue chromophores. More importantly, the conservative limit of 980-nm laser intensity set for human skin exposure is ~0.726 W/cm$^2$, which is more than two times of that (~0.33 W/cm$^2$) of the 808-nm laser (Tian et al. 2011). Therefore, in our experiments, the observations were conducted on a 1-mL solution irradiated by a 980-nm NIR laser at an output power of 0.6 W/cm$^2$. As shown in Fig. 3, with the extension of irradiated time, the temperature increases gradually. After 12-min irradiation, the temperature was enhanced 3.7 °C by Ag/CuS nanocomposites while the temperature was only enhanced 1.4 °C by CuS nanoparticles. In the same period of irradiated time, Ag/CuS always arrives in higher temperature than CuS nanoparticles.

Figures 4 and 5 show fluorescence properties of Ag/CuS nanocomposites and L-ascorbic acid, respectively. Through

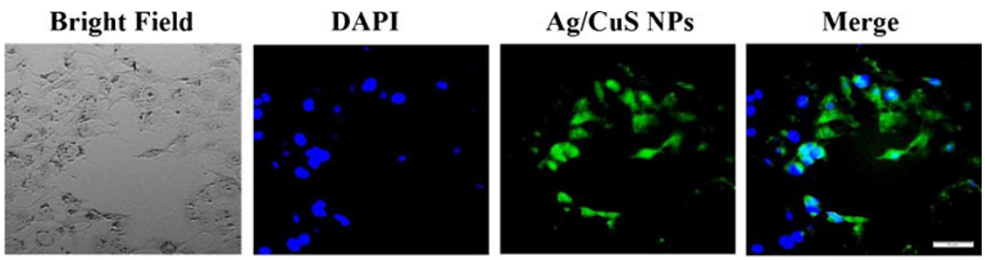


**Fig. 6** The PC-3 prostate cancer cell uptake and imaging of Ag/CuS nanocomposites. The nucleus was stained with DAPI (*blue*) while the green luminescence comes from Ag/CuS nanocomposites. The concentration was 10 % of the original Ag/CuS nanocomposites. *Scale bar*, 50 μm

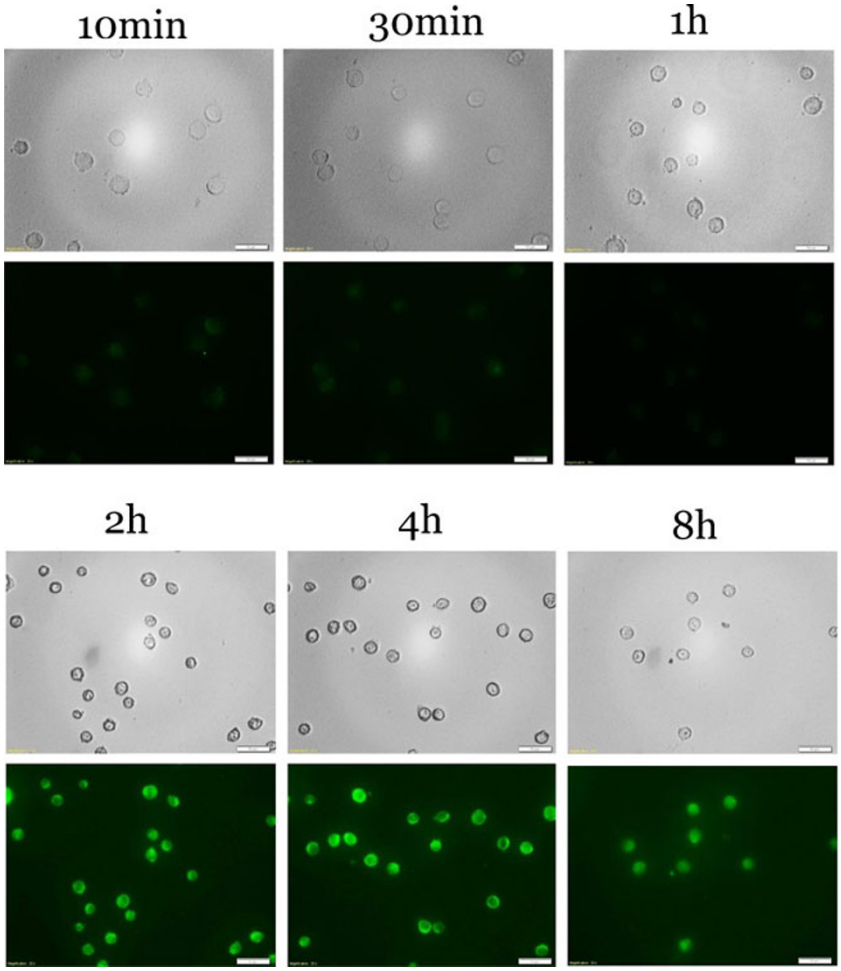


**Fig. 7** The time course of PC-3 cell uptake of Ag/CuS nanocomposites. The *upper images* were taken under bright field; the *lower images* were the fluorescence images of Ag/CuS nanocomposites. The concentration was 5 % of the original Ag/CuS nanocomposites. *Scale bar*, 50 μm

the comparison of excitation and emission spectra in Figs. 4 and 5a, the broad blue–green luminescence peaking at 450 nm is actually derived from the stabilizer ascorbic acid (Guilbault 1990; Wintzinger et al. 2010). Otherwise, in order to further prove the luminescent properties of L-ascorbic acid, the relationship between the emission intensity and the concentration of ascorbic acid is investigated in Fig. 5b, c. The results demonstrate the linear relationship between the emission intensity and the concentration of ascorbic acid. With the concentration of L-ascorbic acid increase, the emission

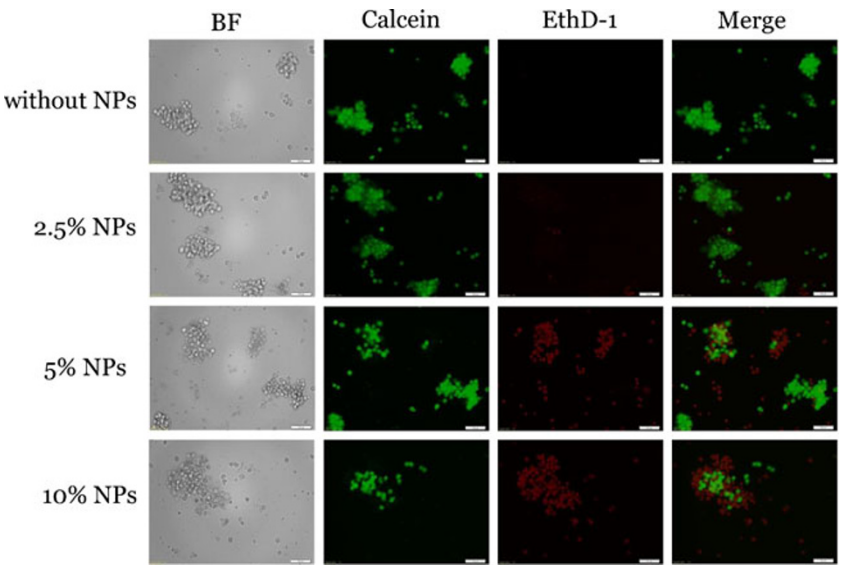


**Fig. 8** Cell viability after 980 nm irradiation. PC-3 prostate cancer cells were treated with different concentrations of Ag/CuS nanocomposites at 0.6 W/cm$^2$ for 5 min. With the increase of concentration of Ag/CuS nanocomposites, more cells were dead. The concentrations are 2.5, 5, and 10 % of the original Ag/CuS nanocomposites. Live cells were stained *green* with calcein AM; dead cells were stained *red* with ethidium homodimer-1 (EthD-1). *Scale bar*, 100 μm

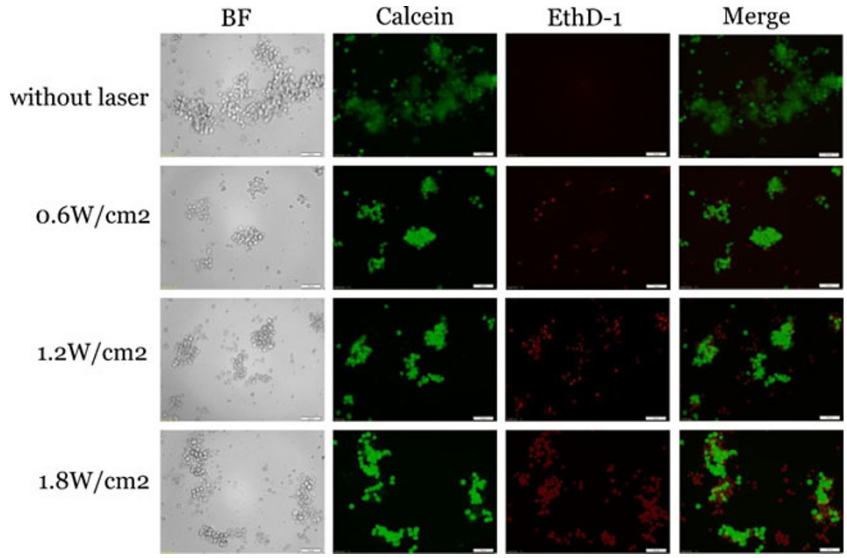


**Fig. 9** Treatment of PC-3 prostate cancer cells with 5 % of original Ag/CuS nanocomposites under different laser power for 5 min. The Ag and Cu concentration of the original Ag/CuS nanocomposites are 13.9 and 46.6 mg/L, respectively. Live cells were stained with calcein AM (*green*); dead cells were stained with EthD-1 (*red*). *Scale bar*, 100 μm

intensity rises. Thus, we infer that L-ascorbic acid indeed has photoluminescence which can be used for cell imaging. Figure 6 shows the uptake of Ag/CuS nanocomposites by PC-3 prostate cancer cells after 24-h incubation. The nucleus of cells was stained with a blue emission dye DAPI. The results show that Ag/CuS nanocomposites can get into PC-3 cells and mainly locate in their cytoplasm. To further observe the cell uptake of these nanocomposites, images were taken for the PC-3 cells treated with Ag/CuS nanocomposites for 10, 30 min, and 1, 2, 3, 4 and 8 h, respectively. The results are shown in Fig. 7. No bright green luminescence is observed in the cells after the incubation less than 1 h. Only after 2-h incubation, luminescence imaging shows that the particles were taken by the cells. As time increasing, the uptake and luminescence intensity are increased and reach the brightest at the 4 h of incubation which means that the cell uptake is saturated. After 8-h incubation, the luminescence is decreased in intensity. This could be due to the loss of the nanocomposites from the cells or the quenching of the ascorbic acid luminescence by the cells. Thus, we may conclude that 4-h incubation is good for cell uptake and treatment.

Figure 8 shows the results of photothermal treatments on PC-3 cells with 980-nm laser at 0.6 W/cm$^2$ for 5 min. Calcein AM is used for visualization of live cells and EthD-1 is for visualization of dead cells. As seen, without nanocomposites all the cells can survive under the laser treatment, while the combination of the laser and the nanocomposites can effectively kill the cancer cells. More and more cells died with the increase of the concentration of nanocomposites at the same laser power and treatment duration. Considering the effective treatment for cancer cells using Ag/CuS nanocomposites dependent on the concentration of nanocomposites, laser power, and treatment duration, the results of the treatment on PC-3 cells at the concentration of 5 % of original Ag/CuS nanocomposites upon the exposure to laser power of 0, 0.6, 1.2, and 1.8 W/cm$^2$ are also carried out in Fig. 9. Without laser, all the cells are alive. More cells were destroyed at the higher laser powers with the same concentration of nanocomposites and treatment duration. Thus, it is concluded that no cancer cells die treated with nanocomposites or laser alone. Only the combination of nanocomposites and laser can kill the cells. The increase of the concentration of Ag/CuS nanocomposites and laser power can induce more cells to die. Here, we have to illustrate the reason why the morphology of the cells in Figs. 6, 7, 8, and 9 look different. In the cell imaging

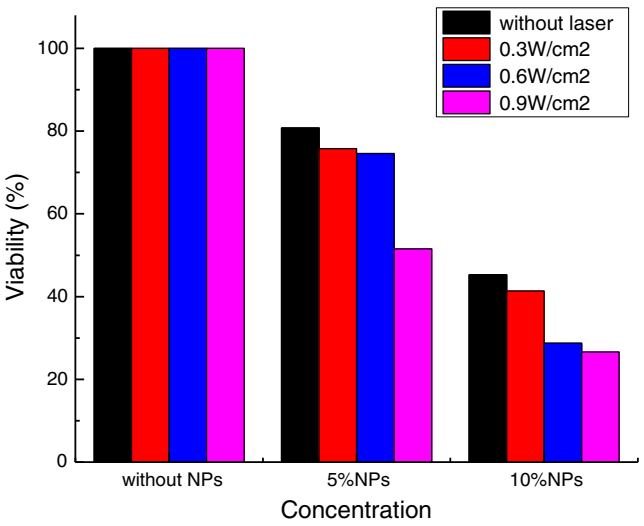


**Fig. 10** Viability of PC-3 cells treated with 5 and 10 % of the original Ag/CuS nanocomposites under different laser power. PC-3 cells without treatment were used as control (not shown in the figure). The Ag and Cu concentration of the original Ag/CuS nanocomposites are 13.9 and 46.6 mg/L, respectively

experiment, in order to locate the Ag/CuS nanocomposites in the cells, the cells should be fixed at the bottom of the cell culture plate. However, considering the possibility of the physical adhesion of Ag/CuS nanocomposites to the culture plate to interfere with the experimental results, the cell cultivation method using EP tubes are utilized in the time course cell uptake. This method is very convenient to use centrifugation to remove all the free particles. However, the disadvantage is to miss the observation of the morphology of cells. While in the photothermal ablation experiments, in order to observe more cells, the biggest scale 100 μm is used rather than 50 μm as before. Thus, due to the different methods and different scales, the morphology of the cells look different.

A quantitative study on the photothermal effect of Ag/CuS nanocomposites was carried out using MTT assay (Fig. 10) for laser output powers of 0, 0.3, 0.6, and 0.9 W/cm$^2$ and nanoparticle concentrations of 5 and 10 %. As a control, the normal cells without nanoparticle and laser treatment represent 100 % viability. The cells treated with lower concentration of Ag/CuS nanocomposites (5 %) have higher viability than those with higher concentration (10 %). With the increase of the laser power, the viability of cells decreases. Without the laser treatment, some cells still died to some extent. It is perhaps due to the existence of CTAB in the nanocomposites (Alkilany and Murphy 2010; Murphy et al. 2008), even though we try to remove all the CTAB using dialysis method.

## 4 Conclusion

Surface plasmon-enhanced photothermal therapy for cancer treatment was investigated in vitro on PC-3 prostate cancer cells using Ag/CuS nanocomposites. The diameters of the Ag/CuS nanocomposites are in the range of 10–20 nm and they have a high absorbance in the near-infrared region. Ag/CuS nanocomposites can get into PC-3 cancer cells and mainly locate in the cytoplasm. The treatment observations found that 5 % of original Ag/CuS nanocomposites activated by a 980 nm laser at 0.6 W/cm$^2$ can efficiently kill cancer cells. With the increase of the nanocomposite concentration or the laser output, more and more cells were killed. Comparing with CuS nanoparticles, surface plasmon-enhanced Ag/CuS nanocomposites have a higher efficiency for the photothermal therapy. It is also a new and promising modality for cancer treatment.

**Acknowledgments** We would like to acknowledge the support from the startup funds from UTA, the NSF and DHS joint ARI program (2011-DN-077-ARI053-03), and the US Army Medical Research Acquisition Activity under contracts of W81XWH-10-1-0279 and W81XWH-10-1-0234. This work was also supported by National Natural Science Foundation of China grant (no. 81072596) and program for New Century Excellent Talents in University (no. NCET-08-0226). At last, we are also grateful for the financial support of China Scholarship Council (no. 2011616067).

## References

Alkilany AM, Murphy CJ (2010) Toxicity and cellular uptake of gold nanoparticles: what we have learned so far? J Nanopart Res 12:2313–2333

Aslan K, Lakowicz JR, Geddes CD (2005) Plasmon light scattering in biology and medicine: new sensing approaches, visions and perspectives. Curr Opin Chem Biol 9:538–544

Castrén-Persons M, Schröder T, Rämö OJ, Puolakkainen P, Lehtonen E (1991) Contact Nd:YAG laser potentiates the tumor cell killing effect of hyperthermia. Lasers Surg Med 11:595–600

Chen WR, Adams RL, Carubelli R, Nordquist RE (1997) Laser-photosensitizer assisted immunotherapy: a novel modality for cancer treatment. Cancer Lett 115:25–30

Chen J, Wiley B, Li ZY, Campbell D, Saeki F, Cang H, Au L, Lee J, Li X, Xie Y (2005) Gold nanocages: engineering their structure for biomedical applications. Adv Mater 17:2255–2261

Dickerson EB, Dreaden EC, Huang X, El-Sayed IH, Chu H, Pushpanketh S, McDonald JF, El-Sayed MA (2008) Gold nanorod assisted near-infrared plasmonic photothermal therapy (PPTT) of squamous cell carcinoma in mice. Cancer Lett 269:57–66

El-Sayed IH, Huang X, El-Sayed MA (2006) Selective laser photothermal therapy of epithelial carcinoma using anti-EGFR antibody conjugated gold nanoparticles. Cancer Lett 239:129–135

Englebienne P, Hoonacker AV, Verhas M (2003) Surface plasmon resonance: principles, methods and applications in biomedical sciences. Spectroscopy 17:255–273

Evanoff DD Jr, Chumanov G (2005) Synthesis and optical properties of silver nanoparticles and arrays. Chem Phys Chem 6:1221–1231

Feng X, Ruan F, Hong R, Ye J, Hu J, Hu G, Yang Z (2011) Synthetically directed self-assembly and enhanced surface-enhanced Raman scattering property of twinned crystalline Ag/Ag homojunction nanoparticles. Langmuir 27:2204–2210

Guilbault GG (1990) Assay of organic compounds. In: Guilbault GG (ed) Practical fluorescence, 2nd edn. Marcel Dekker, New York, pp 337–338

Hu M, Petrova H, Chen J, McLellan JM, Siekkinen AR, Marquez M, Li X, Xia Y, Hartland GV (2006) Ultrafast laser studies of the photothermal properties of gold nanocages. J Phys Chem B 110:1520–1524

Huang X, El-Sayed MA (2011) Plasmonic photo-thermal therapy (PPTT). Alex J Med 47:1–9

Huang X, Jain PK, El-Sayed IH, El-Sayed MA (2006a) Determination of the minimum temperature required for selective photothermal destruction of cancer cells using immunotargeted gold nanoparticles. Photochem Photobiol 82:412–417

Huang X, EI-Sayed IH, Qian W, EI-Sayed MA (2006b) Cancer cell imaging and photothermal therapy in the near-infrared region by using gold nanorods. J Am Chem Soc 128:2115–2120

Huang X, Jain PK, El-Sayed IH, El-Sayed MA (2008) Plasmonic photothermal therapy (PPTT) using gold nanoparticles. Lasers Med Sci 23:217–228

Huff TB, Tong L, Zhao Y, Hansen MN, Cheng JX, Wei A (2007) Hyperthermic effects of gold nanorods on tumor cells. Nanomedicine 2:125–132

Khlebtsov B, Zharov V, Melnikov A, Tuchin V, Khlebtsov N (2006) Optical amplification of photothermal therapy with gold nanoparticles and nanoclusters. Nanotechnology 17:5167–5179

Kim SJ, Stach EA, Handwerker CA (2012) Silver layer instability in a SnO2/Ag/SnO2 trilayer on silicon. Thin Solid Films 520:6189–6195

Lakowicz JR (2001) Radiative decay engineering: biophysical and biomedical applications. Anal Biochem 298:1–24

Lakshmanan SB, Zou X, Hossu M, Ma L, Yang C, Chen W (2012) Local field enhanced Au/CuS nanocomposites as efficient

photothermal transducer agents for cancer treatment. J Biomed Nanotechnol 8:1–8

Li JL, Gu M (2010) Gold-nanoparticle-enhanced cancer photothermal therapy. IEEE J Sel Top Quant Electron 16:989–996

Li Y, Lu W, Huang Q, Huang M, Li C, Chen W (2010) Copper sulfide nanoparticles for photothermal ablation of tumor cells. Nanomedicine 5:1161–1171

Loo C, Lowery A, Halas NJ, West JL, Drezek R (2005) Immunotargeted nanoshells for integrated cancer imaging and therapy. Nano Lett 5:709–711

Murphy CJ, Gole AM, Stone JW, Sisco PN, Alkilany AM, Goldsmith EC, Baxter SC (2008) Gold nanoparticles in biology: beyond toxicity to cellular imaging. Acc Chem Res 41:1721–1730

O'Neal DP, Hirsch LR, Halas NJ, Payne JD, West JL (2004) Photothermal tumor ablation in mice using near infrared-absorbing nanoparticles. Cancer Lett 209:171–176

Rau B, Wust P, Tilly W, Gellermann J, Harder C, Riess H, Budach V, Felix R, Schlag PM (2000) Preoperative radiochemotherapy in locally advanced or recurrent rectal cancer: regional radiofrequency hyperthermia correlates with clinical parameters. Int J Radiat Oncol Biol Phys 48:381–391

Robinson JT, Welsher K, Tabakman SM, Sherlock SP, Wang H, Luong R, Hongjie D (2010) High performance in vivo near-IR (>1 μm) imaging and photothermal cancer therapy with carbon nanotubes. Nano Res 3:779–793

Rozanova N, Zhang J (2009) Photothermal ablation therapy for cancer based on metal nanostructures. Sci China Ser B Chem 52:1559–1575

Sharma S, Ahmad N, Prakash A, Singh VN, Ghosh AK, Mehta BR (2010) Synthesis of crystalline Ag nanoparticles (AgNPs) from microorganisms. Mater Sci Appl 1:1–7

Sohrabnezhad S, Pourahmad A (2012) As-synthesis of nanostructure AgCl/Ag/MCM-41 composite. Spectrochim Acta A Mol Biomol Spectrosc 86:271–275

Song CW, Shakil A, Osborn JL, Iwata K (1996) Tumour oxygenation is increased by hyperthermia at mild temperatures. Int J Hyperther 12:367–373

Sun Z, Yang Z, Zhou J, Yeung MH, Ni W, Wu H, Wang J (2009) A general approach to the synthesis of gold-metal sulfide core–shell and heterostructures. Angew Chem 121:2925–2929

Svaasand LO, Gomer CJ, Morinelli E (1990) On the physical rationale of laser induced hyperthermia. Lasers Med Sci 5:121–128

Tian Q, Tang M, Sun Y, Zou R, Chen Z, Zhu M, Yang S, Wang J, Wang J, Hu J (2011) Hydrophilic flower-like CuS superstructures as an efficient 980 nm laser-driven photothermal agent for ablation of cancer cells. Adv Mater 23:3542–3547

Wintzinger L, An W, Turner CH, Bao Y (2010) Synthesis and modeling of fluorescent gold nanoclusters. Joshua 7:24–27

Wu C, Yu S-H, Chen SF, Liu GN, Liu BH (2006) Large scale synthesis of uniform CuS nanotubes in ethylene glycol by a sacrificial templating method under mild conditions. J Mater Chem 16:3326–3331

Xu HL, Wang Z, Zhu W (2006) Sonochemical synthesis of crystalline CuS nanoplates via an in situ template route. Mat Lett 60:2203–2206

Zee JVD (2002) Heating the patient: a promising approach? Ann Oncol 13:1173–1184

Zhou F, Xing D, Ou Z, Wu B, Resasco DE, Chen WR (2009) Cancer photothermal therapy in the near-infrared region by using single-walled carbon nanotubes. J Biomed Opt 14:021009

Zhou M, Zhang R, Huang M, Lu W, Song S, Melancon MP, Tian M, Liang D, Li C (2010) A chelator-free multifunctional [$^{64}$Cu]CuS nanoparticle platform for simultaneous micro-PET/CT imaging and photothermal ablation therapy. J Am Chem Soc 132:15351–15358

Zhu HL, Ji X, Yang D, Ji Y, Zhang H (2005) Novel CuS hollow spheres fabricated by a novel hydrothermal method. Microporous Mesoporous Mater 80:153–156